

This is the peer reviewed version of the following article:

Garcias J. F., Martins R. F., Branco R., Marciniak Z., Macek W., Pereira C., Santos C., Quasistatic and fatigue behavior of an AISI H13 steel obtained by additive manufacturing and conventional method, *FATIGUE & FRACTURE OF ENGINEERING MATERIALS & STRUCTURES*, Vol. 44, iss. 12 (2021), pp.3384-3398, which has been published in final form at <https://dx.doi.org/10.1111/ffe.13565>.

This article may be used for non-commercial purposes in accordance with Wiley Terms and Conditions for Use of Self-Archived Versions. This article may not be enhanced, enriched or otherwise transformed into a derivative work, without express permission from Wiley or by statutory rights under applicable legislation. Copyright notices must not be removed, obscured or modified. The article must be linked to Wiley's version of record on Wiley Online Library and any embedding, framing or otherwise making available the article or pages thereof by third parties from platforms, services and websites other than Wiley Online Library must be prohibited.

Quasi-static and fatigue behaviour of an AISI H13 steel obtained by additive manufacturing and conventional method

Journal:	<i>Fatigue & Fracture of Engineering Materials & Structures</i>
Manuscript ID	FFEMS-9422.R1
Wiley - Manuscript type:	Original Article
Date Submitted by the Author:	n/a
Complete List of Authors:	Garcias, José; New University of Lisbon Faculty of Science and Technology Martins, Rui; UNIDEMI, New University of Lisbon, Nova School of Science and Technology, Department of Mechanical and Industrial Engineering Branco, Ricardo; Universidade de Coimbra Faculdade de Ciências e Tecnologia, Department of Mechanical Engineering Marciniak, Zbigniew; Opole University of Technology Faculty Of Mechanical Engineering Macek, Wojciech; Institute of Chemical Engineering of the Polish Academy of Sciences, Pereira, Cândida; Polytechnic Institute of Leiria Centre for Rapid and Sustainable Product Development Santos, Cyril; Polytechnic Institute of Leiria Centre for Rapid and Sustainable Product Development

SCHOLARONE™
Manuscripts

Quasi-static and fatigue behaviour of an AISI H13 steel obtained by additive manufacturing and conventional method

José F. Garcias¹, Rui F. Martins^{1,*}, Ricardo Branco², Zbigniew Marciniak³, Wojciech Macek⁴,
Cândida Pereira⁵, Cyril Santos⁵

¹UNIDEMI, Department of Mechanical and Industrial Engineering, Nova School of Science and Technology,
Campus de Caparica, Universidade NOVA de Lisboa, 2829-516 Caparica – Portugal

²Department of Mechanical Engineering, CEMMPRE, University of Coimbra, Rua Luís Reis Santos, Pinhal de
Marrocos, 3030-788 Coimbra – Portugal

³Opole University of Technology, Faculty of Mechanical Engineering, Mikolajczyka 5, 45-271 Opole – Poland

⁴Gdańsk University of Technology, Faculty of Mechanical and Ocean Engineering, 11/12 Gabriela
Narutowicza, Gdańsk, 80-233, Poland

⁵Centre for Rapid and Sustainable Product Development, Polytechnic Institute of Leiria, Rua de Portugal,
Marinha Grande, 2430-028 - Portugal

Abstract

This work aims to compare the mechanical behaviour of an AISI H13 steel obtained by additive manufacturing with that obtained by conventional manufacturing methods. The average values of the ultimate tensile strength (UTS) and ductility obtained for the specimens produced by the conventional method were equal to 658 MPa and 18%, respectively, which compares with 503 MPa and 0.75% registered for the SLM specimens. Inversely, the average hardness value determined for the SLM specimens was higher, 450HV, than the observed for the conventional, 200 HV. In addition, the maximum applied stress corresponding to a fatigue limit's endurance of 2×10^6 cycles was equal to 340 MPa and 85 MPa for conventional and SLM specimens, respectively. Therefore, from a fatigue design point of view, it was possible to infer that $\sigma_{\max}/UTS=0.17$ for the SLM specimens tested. Porosity and lack of fusion influenced the static and the fatigue strength negatively in the SLM specimens.

Keywords: AISI H13; Powder Bed Fusion; Selective Laser Melting (SLM); Mechanical Properties.

1. Introduction

Additive Manufacturing (AM) is a technology based on the addition of material instead of its removal, aiming to become increasingly more eco-efficient and sustainable. It is used for the manufacture of parts by overlapping layers of material from a 3D CAD model, and, currently, the most common methods to produce metal objects in AM are powder bed fusion, where SLM is included, direct energy deposition, binder jetting, and sheet lamination¹. Initially used in the prototyping of individual parts, this process has become relevant in the manufacture of final functional products due to the advances made in this area. In fact, the ability to produce metallic products has had a significant impact on the industry since the 1990s, making it possible to manufacture complex geometry components with mechanical, thermal, and electrical properties that polymeric materials do not have²⁻⁴. Moreover, the

Selective Laser Melting (SLM) manufacturing process can produce parts by melting and consequent solidification of successive layers of metallic powder using a laser as an energy source^{5,6}. This process is used, among others, in the manufacture of moulds and dies^{7,8}, and according to a 2019 market report⁹, metal AM is expected to generate \$228 billion worth of components this decade and is expected to shift from a prototype technology to a dominant production industry by the end of 2022.

Concerning the AISI H13 steel, it is considered a hot-working steel usually used to manufacture metal components subjected to high temperatures. This material has excellent resistance to thermal fatigue, erosion, and wear, and is often used to produce moulds and dies using SLM¹⁰.

The paper's primary objective is to compare the static and the mechanical fatigue behaviour of an AISI H13 steel obtained by additive manufacturing with that obtained by conventional manufacturing methods. Moreover, in this research, we were interested in determining the mechanical properties of this 3D printed steel without undergoing thermal treatments to establish new application fields in which the steel could be directly applied in the as-printed condition.

Following the introduction, the paper is organised as follows: Section 2 presents data on AISI H13 steel, Section 3 describes the materials and methods used for this research; Section 4 gathers information on the experimental tests carried out, results and discussion. The paper ends with a summary of the most relevant findings.

2. Literature data on AISI H13 steel

The AISI H13 steel is an ultra-high strength steel, which, depending on the thermal treatments applied, can attain a maximum ultimate tensile strength near 2000 MPa¹¹ and hardness values ranging from 28 to 52 HRC (see Table 1).

Table 1 – Mechanical properties of conventional AISI H13 steel obtained from an initial temperature of 1010°C, followed by oil-quenching and a dwell period of 2 hours at different tempering temperatures (adapted from¹¹).

Tempering temperature [°C]	Tensile Strength, UTS [MPa]	Yield Strength, YS [MPa]	Elongation %	Charpy V-notch impact energy [J]	Hardness [HRC]
527	1960	1570	13	16	52
555	1835	1530	13.1	24	50
575	1730	1470	13.5	27	48
593	1580	1365	14.4	28.5	46
700	-	-	-	-	28

Ruhi Yeşildal¹² studied the fatigue limit of conventional AISI H13 steel, correspondent to an endurance of 1×10^6 cycles, in function of different thermal treatments, and concluded that it varied significantly, with a minimum value of 470 MPa in case of no thermal treatments were applied.

However, the mechanical properties of the components obtained through metallic powder bed manufacturing methods, strongly depend on the material's characteristics and the process parameters¹³. One of the most significant parameters in the SLM process is the energy delivered to the material, heat input, which affects the melting pool characteristics and, consequently, the final component's properties. This energy is referred to as energy density, E , and can be described by:

$$E \left[\frac{J}{mm^3} \right] = \frac{P [W]}{v \left[\frac{mm}{s} \right] \cdot h [mm] \cdot t [mm]} \quad (1)$$

where P is the laser power [W], v is the laser scanning speed [mm/s], h represents the hatch spacing [mm], and t is the layer thickness [mm]¹⁴.

The value of the energy density (E) depends on the base material's properties, being necessary to optimize the process conditions for each material. When E is superior to the optimum conditions, the melting pool becomes unstable, which can cause porosity and poor surface finish; on the other hand, if E is less than optimal conditions, it can lead to the appearance of defects related to the lack of fusion. Thus, any change in the parameters P , v , h , and t influences the energy density and, in turn, the components' mechanical properties.

Lee *et al.*¹⁵ obtained increasing porosity values, namely 0.3%, 1% and 3% for successively higher laser scanning speed values - 200, 400 and 800 mm/s, respectively, and, in accordance, Deirmina *et al.*¹⁶ concluded that there is a decrease in the porosity of the components obtained for higher values of energy density. Moreover, from the study of Lee *et al.*¹⁵, the following conclusions could be drawn for the AISI H13 steel obtained through SLM (Table 2):

- The hardness values decreased as the laser speed increased;
- The yield stresses obtained in the three cases are similar; however, it is noteworthy that the tensile strength is considerably higher in the specimen obtained with a lower laser speed (200 mm/s).
- The ductility is also notably more significant in the material obtained at the lower laser speed (200 mm/s).

Table 2 – Mechanical properties of AISI H13 steel for three laser speeds (SLM) (adapted from¹⁵).

Specimens	Yield Strength, YS [MPa]	Tensile Strength, UTS [MPa]	Elongation [%]	Vickers hardness (HV)
200 mm/s	1342±67	1704±30	1.55±0.05	585
400 mm/s	1167±73	1321±11	0.35±0.05	516
800 mm/s	1133±42	1227±46	0.30±0.10	469

Considering the effect of thermal treatments, Yan *et al.*⁶ studied the effect of performing tempering treatments at two different temperatures on the material's mechanical properties. The values of YS, UTS, extension and hardness are shown in Table 3, where it is possible to conclude that the ductility increased with the tempering temperature. YS, UTS and material hardness were maximum for the treatment performed at 600 °C and decreased considerably when performed at 700 °C. These values are also in agreement with the tendency shown in Table 1.

Table 3 – Mechanical properties of AISI H13 steel obtained by SLM in the as printed condition and after the application of thermal treatments (adapted from⁶).

Samples	Yield Strength, YS [MPa]	Tensile Strength, UTS [MPa]	Elongation [%]	Vickers hardness (HV)
As-printed	818±12	1430±12	2.42±0.21	565±7.4
600°C tempering	1483±48	1938±62	5.8±0.61	629±10.1
700°C tempering	877±18	1076±21	10.95±1.68	371±10.6

In addition, the experimental work carried out by Nagahama *et al.*¹⁷ allowed comparing the mechanical properties of an AISI H13 steel obtained by SLM for two manufacturing orientations, 0° (horizontal) and 90° (vertical), through uniaxial tensile tests. Based on the data obtained, the authors concluded that the manufacturing orientation significantly affects mechanical properties. Regarding

tensile strength, they observed that for the manufacturing orientation at 0° , the value was much higher (1570 MPa) than that obtained at 90° (1050 MPa).

The literature results are very limited in the fatigue resistance of additively manufactured AISI H13 steel. Nevertheless, a recent investigation carried out by Dörfert *et al.*¹⁸ allowed to determine a fatigue limit of 283 MPa for a load ratio, R , equal to -1, and for machined specimens of AM AISI H13 steel. Besides, when considering the as-built specimens, without turning, the fatigue limit obtained for the same testing conditions lowered below 100 MPa. Hence, the worse surface finish inherent to the SLM process must be improved through machining and polishing to enhance fatigue resistance of functional components obtained by additive manufacturing.

In order to fill the above gaps, the present work aims at studying the mechanical behaviour of a AISI H13 steel manufactured by SLM, with emphasis on the fatigue response. The results will be compared with those of conventional AISI H13 steel.

3. Materials and methods

This section describes the process conditions and parameters defined in the specimens' manufacture by SLM, as well as the entire experimental procedures carried out to characterize the mechanical properties of the material under study.

3.1 Metal powder and SLM parameters

The metallic powder used in the specimens manufactured by SLM had dimensions comprehended between 10 and 45 μm and was purchased to SLM SOLUTIONS. Its chemical composition, in weight percentage, is described in Table 4¹⁹.

Table 4 – Chemical composition of the metallic powder used in the production of the SLM specimens.

	Fe	C	Cr	Mn	Mo	Ni+Cu	P	S	Si	V
AISI H13	Bal.	0.32-	4.75-	0.20-	1.10-	0.75	0.03	0.03	0.80-	0.8-
(10-45 μm)		0.45	5.50	0.60	1.75				1.25	1.20

The Centre for Rapid and Sustainable Product Development of the Polytechnic Institute of Leiria produced the additively manufactured specimens using an SLM 125 machine from SLM SOLUTIONS. The process parameters are presented in Table 5. E refers to the energy density, P represents the laser's power, e is the thickness of the layer, h is the hatch spacing, and v is the laser beam speed. After printed, the specimens were machined and successively polished with P300, P500, P1000, P1500, P2000 and P2500 sandpaper, and, in the end, with 6 μm diamond paste, without having undergone any thermal treatments. The test pieces were manufactured vertically, with the manufacturing orientation at 90° . Figure 1a illustrates a specimen obtained by SLM already machined and polished. The specimens obtained by conventional methods, illustrated in Figure 1b, were machined by a CNC lathe, from a 20 mm thick plate, without subsequent polishing. The test pieces were not subjected to thermal treatments.

Table 5 - Process conditions and parameters used to print SLM specimens.

Regions	E [J/mm ³]	P [W]	e [mm]	h [mm]	v [mm/s]
Interior	111.11	100	0.03	0.12	250
Contour	92.59	100	0.03	0.12	300

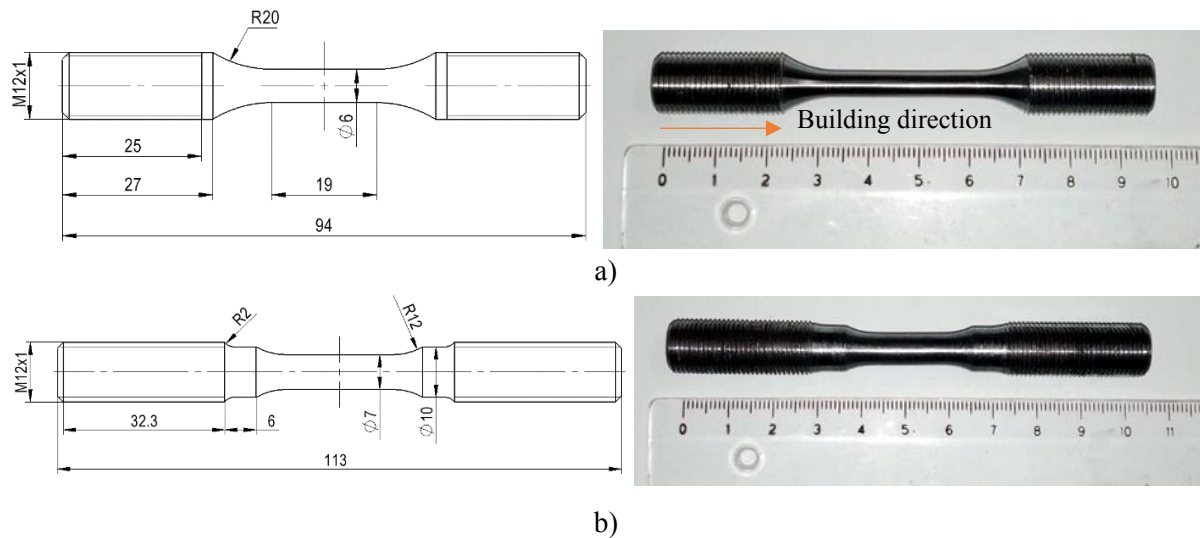


Fig. 1 – Specimens: overall view and dimensions (unit: mm). a) SLM; and b) Conventional.

The SLM specimen was designed using the Finite Element Method (FEM) to maximise the stresses present at reduced section, minimise weight, and, consequently, the quantity of metal powder used during the additive manufacturing process.

3.2 Surface roughness

To measure the surface roughness, three readings were performed on each specimen before the experimental tests with the following process parameters: L_t represents the traversing length (3 mm), L_c the individual reading length (0.25 mm), N the number of sampling lengths (5), M_s the measuring speed (0.5 mm/s) and P_t the Probe type (0.35 mm). The equipment used was a Mahr MarSurf PS 10 rugosimeter.

3.3 Micrographs

Two samples were prepared with the central section of the SLM and conventional specimens, which were embedded in resin and successively subjected to P80, P240, P320, P400, P600, P1200, P2500 sandpaper and finally polished with a diamond paste of 3 μm , to carry out the microscopic analysis. The samples were etched with Nital 5%. The microstructure was examined using an Olympus CX40 microscope and an Olympus DP21 capture camera.

3.4 Microhardness measurements

The Vickers microhardness was measured along the samples' diameter, as shown in Figures 2 a,b), where the cross-section to each specimen's manufacturing orientation is shown. The indentations were spaced 0.25 mm apart, as indicated by the ASTM E384 standard²⁰. The Mitutoyo HM-100 equipment was used, applying 1000 gf for 10 seconds. Hardness was read in samples manufactured by conventional method (Fig. 2a) and SLM (Fig. 2b) processes. The microhardness measurement of an SLM sample was also performed for a section perpendicular to the manufacturing orientation, along a vertical line and a horizontal line, as illustrated in Figure 2c).

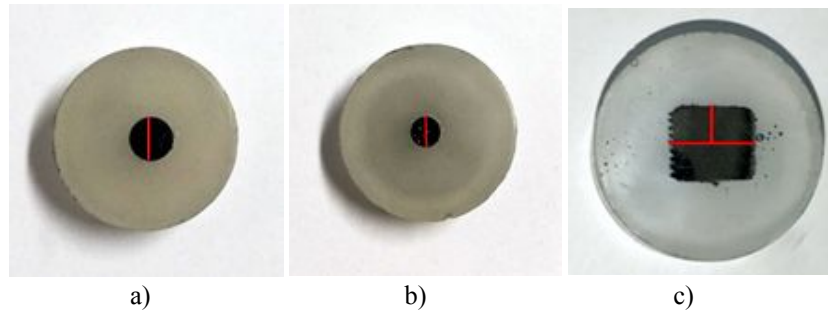


Fig. 2 – Microhardness measurements of a) transversal cross-section of conventional steel; b) transversal cross-section of SLM specimen; and c) longitudinal cross-section of SLM specimen.

3.5 Uniaxial tensile tests

Six specimens were randomly selected, three obtained by SLM and the other three manufactured by conventional processes. The uniaxial traction tests were carried out in the Department of Mechanical and Industrial Engineering of Nova School of Science and Technology (FCT-UNL) on a servohydraulic machine MTS Model 312.21 with a load cell of 100 kN. The transducer used to monitor displacement was the MTS Model 632.12C-21. The tests were carried out at room temperature, with a gradual increase in the applied force with the moorings' displacement speed defined in 0.02 mm/s.

3.6 Uniaxial fatigue tests

The H13 specimens obtained through conventional manufacturing methods were tested at FCT-UNL (Portugal), using a servohydraulic machine for uniaxial tensile tests. The H13 samples produced by SLM were tested at Science and Technology Park in Opole (Poland) using a Instron testing machine, Model No. 8802, MTB 13127, with a maximum load cell of 100 kN. The tests on specimens obtained by conventional methods were carried out at a frequency of 3 Hz, with the load ratio value, R , set at approximately $R = 0.2$. The SLM specimens' tests were performed at a load ratio $R = 0.2$ and a frequency of 1 Hz for the highest load values, 2 Hz for the intermediate load level, and 5 Hz for the load level at which it was expected to reach infinite life. All tests were carried out at room temperature. Considering the Japan Society of Mechanical Engineers (JSME)²¹, two specimens were used for each load level, for at least four different stress levels in the finite life region. Test pieces that reached two million cycles were considered infinite life (Run Out). The high-stress ratio value was chosen to minimise fatigue life. In addition, the low testing frequency was defined to assure that the servohydraulic machine really applied the imposed loading.

3.7 Analysis of fracture surfaces

The fracture surfaces resultant from the tensile and fatigue tests were analysed using the Hitachi S2400 Analytical Scanning Electron Microscope (SEM). Besides, the initiation of cracks and their mechanisms of propagation were also identified. In addition, the failed specimens were also observed under specific magnification using an Alicona G4 Infinite Focus as described elsewhere²².

4. Results and discussion

This section focuses on the results obtained during the experimental procedure and their analysis.

4.1 Surface roughness

The surface finish substantially affects the fatigue resistance of mechanical components. Considering the average roughness values measured on the specimens under study (Table 6), it was possible to infer a correction factor for the fatigue limit due to the surface finish of approximately 0.9 for SLM specimens and approximately 0.76 for conventional manufacture²³.

Table 6 - Average roughness values measured on the specimens under study.

	Ra (μm)	Rq (μm)
Conventional methods	1.130	1.458
SLM	0.172	0.342

4.2 Micrographic Analysis

As mentioned in section 3.3, etching was carried out on SLM manufacture samples and conventional manufacture with Nital 5%. The chemical attack revealed the microstructure of the sample obtained by conventional methods. However, even with a significant increase in nitric acid concentration up to 11%, it was impossible to reveal the SLM sample's microstructure. The chemical attack carried out on the AISI H13 samples obtained by conventional methods can be seen in Figures 3 a) and b), where it is possible to observe the martensitic microstructure with carbides' deposition (darker points)²⁴.

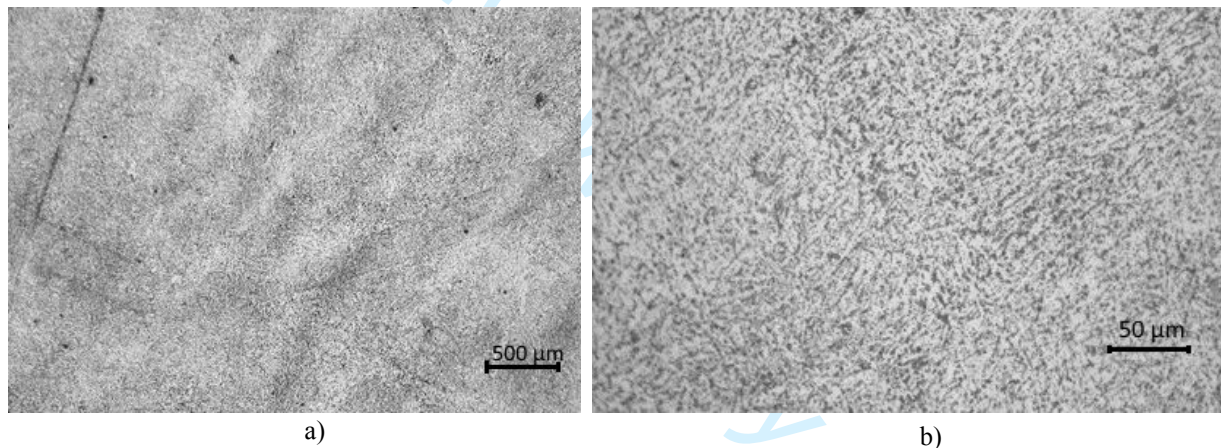


Fig. 3 – The microstructure of AISI H13 steel obtained by conventional methods with a magnification of a) 20x; and b) 100x.

Although it was not possible to reveal the microstructure of the H13 steel obtained by SLM, the chemical attack made it possible to observe the laser's trajectory in the specimen body and in the region closest to the outer surface, as well as some defects (Fig. 4). It was observed that a cross scan strategy was used in the specimen's body, that is, with passages perpendicular to each other, as shown in Figures 4 a, b), and, in the region closest to the outer surface, a circular scan strategy was performed throughout the entire sample, as illustrated in Figure 4 c). In Figure 4e), the presence of several porosities between two scans tracks is visible, which may occur due to their lack of overlap. This defect can lead to the appearance of a crack, as shown in Figure 4d). It is also important to highlight pores of reduced dimensions, less than 200 μm , close to the outer surface, which represent possible points of crack initiation when subjected to fatigue loading. Simultaneously, a lack of fusion was detected. Therefore, it is concluded that the process parameters used were not ideal and negatively affected the characteristics of the melting pool, resulting in a final product with a density considerably lower than expected. In fact, for the SLM process parameters used (Table 5) and for the energy density values to which the material was theoretically subjected ($>100 \text{ J/mm}^3$), it would be expected to obtain a percentage of defects below 2%^{14, 25}. Nevertheless, higher values of defects were obtained ($\cong 8\%$). This porosity percentage was calculated from the analysis of transversal and longitudinal cross-sections (micrographs) taken out from

two specimens (Figures 2 and 4). The total area of the pores, visible in each micrograph analysed, was determined by the summation of each pore's area, and related to the total cross-section area observed as if it were 100% dense (percentage).

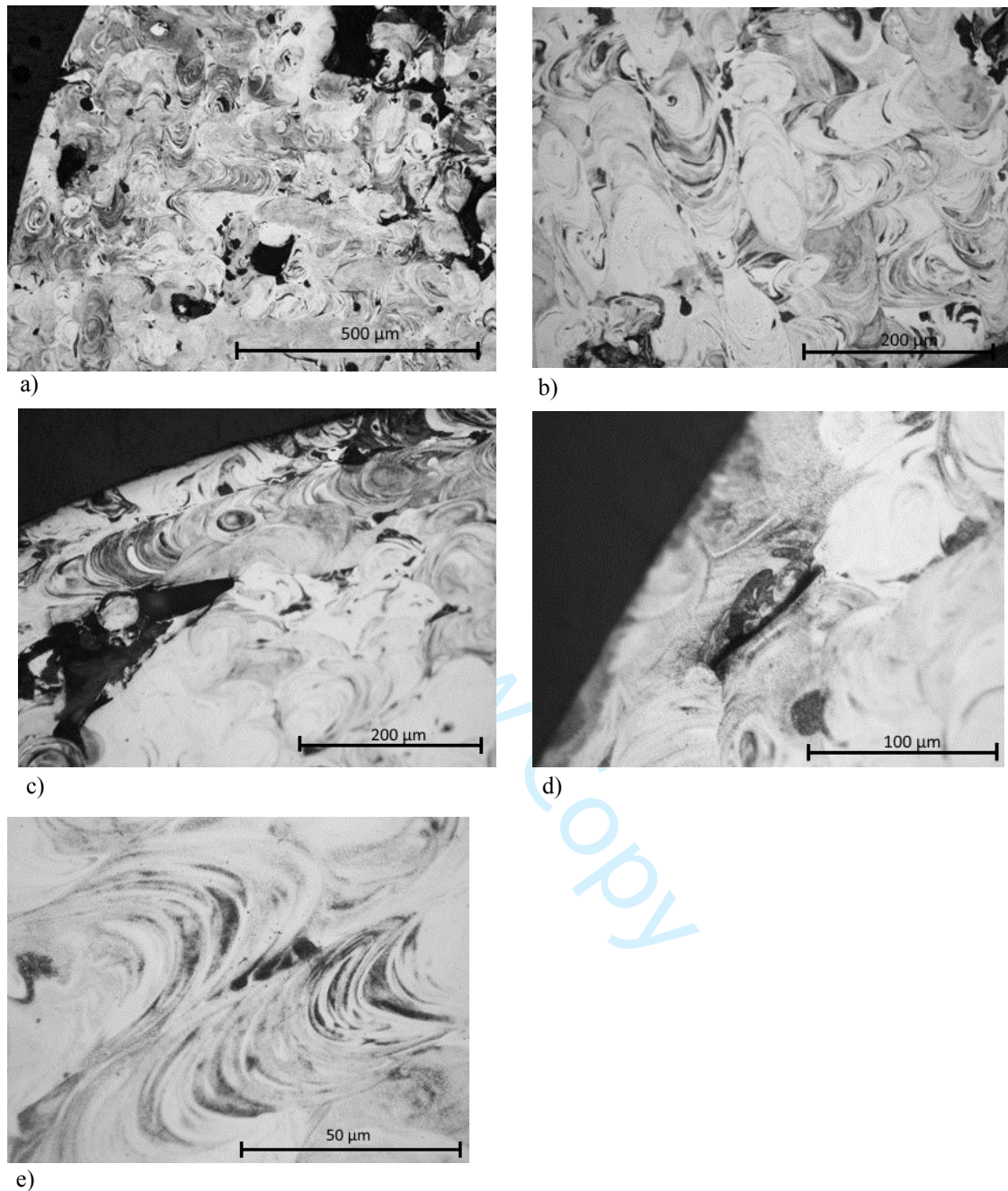


Fig. 4 – Microscopic view of the cross section of a SLM specimen etched with Nital 11% with magnification of a) 10x; b) 20x; c) 20x; d) 50x; and e) 100x.

4.3 Hardness tests

The hardness tests were carried out to compare the two manufacturing methods and their effect on the mechanical properties. The results show that the SLM samples' hardness values are higher than those obtained in the conventionally manufactured samples. For the SLM samples, a maximum value of 540.7 HV and a minimum of 317.2 HV were determined, while for the conventional specimens, a maximum value of 218 HV and a minimum of 176.4 HV were obtained.

The variation in the SLM samples' measurements is due to porosity in the regions where the indentations were made. This variation is lower in samples of conventional manufacture, which have a negligible percentage of defects. Moreover, the maximum values obtained in the SLM specimens are close to the outer surfaces due to the higher cooling rates to which the regions are subjected, which dissipate heat more quickly to the outside environment and the shielding gas; simultaneously, this phenomenon can also be affected by the plastic deformation induced by the machining and polishing process of the outer surface of the test pieces. In addition, the central areas of the SLM specimens are subjected to multipass, with several thermal cycles, lower cooling rates, dissipating heat to the surrounding material, and inducing an annealing process that decreases its hardness.

For process parameters like those used in the manufacture of SLM specimens, according to the studies mentioned in Section 2, average values between 516-585 HV were expected¹⁵, with the respective standard deviation between 7.4-18 HV. The results obtained show that the average value obtained ($450\text{HV} \pm 48$) is lower than foreseen; however, the maximum values are comparable (509-540 HV). The significantly higher standard deviation is due, as explained above, to the effect of defects on hardness measurements. In fact, in the Vickers hardness test, the indentation of an SLM cross-section could occur in the vicinity of pores, originating greater impression diagonal lengths due to the higher deformation of the non-supported material, resulting in lower local hardness values.

Regarding the results obtained for samples manufactured by conventional methods, the values are lower than those usually reported and used in the industry. However, when the material is not subjected to any heat treatment, hardness values in the observed range are expected²⁶.

4.4 Uniaxial tensile tests

Concerning the results of specimens manufactured by conventional methods, a maximum value of 662 MPa was obtained for UTS and a maximum value of 21% for ductility (Table 7). The strain values are similar to those described in Section 2, confirming this material's high ductility. The value obtained for the UTS is lower than expected, with a reduction of approximately 58% when compared to the 1590 MPa reported in the literature²⁷. However, the higher value outlined resulted from applying a tempering treatment, which was not the case of the conventional specimens under study. Moreover, the hardness values measured were lower (section 4.3), thus reducing the tensile strength.

Regarding the SLM test pieces' results, a maximum value of 513 MPa was obtained for the UTS and a value of 0.75% for the ductility (Table 7). The UTS value is significantly lower (-48.7%) than the reference value for 90° SLM manufacture, approximately 1000 MPa (Section 2 and Table 7¹⁷). The strain at rupture is comparable to the values obtained by other authors, such as Lee *et al.*¹⁵, for similar manufacturing parameters and without performing thermal treatments or stress relief.

Table 7 - Results of tensile tests for tensile strength (UTS) and rupture strain.

Specimen ref.	Tensile Strength, UTS [MPa]	Rupture Strain [%]
Conventional (A14)	659	21
Conventional (A12)	652	14
Conventional (A11)	662	18,4
SLM (B11)	504	n.d.
SLM (C4)	493	0.75
SLM (C2)	513	n.d.
Conventional reference value ²⁷	1350-1590	>13
SLM reference value at 0° ²⁸	1712	4.1 ± 1.2
SLM reference value at 90° ¹⁷	1000	N.D

Furthermore, it has been experimentally proven that the presence of defects to values higher than those considered acceptable for an optimized process (maximum of 2%) can reduce up to approximately

79% the value of UTS (with 45% of defects for a Ti-6Al-4V alloy obtained by SLM)²⁹. Similarly, the rupture strains' values are critically affected by the presence of defects, and up to approximately 64% of reduction was observed for an AISI 316L steel obtained by SLM with 16% defects^{30, 31}.

In addition, it was observed on the fracture surface of the specimens obtained by SLM that the deformation before the fracture is minimal, illustrated in Figure 5a), typical of a brittle fracture. On the other hand, in specimens obtained by conventional manufacture, it was noted that there was much deformation before the fracture, with a significant reduction in area. This behaviour is characteristic of a ductile fracture and is shown in Figures 5b, c).

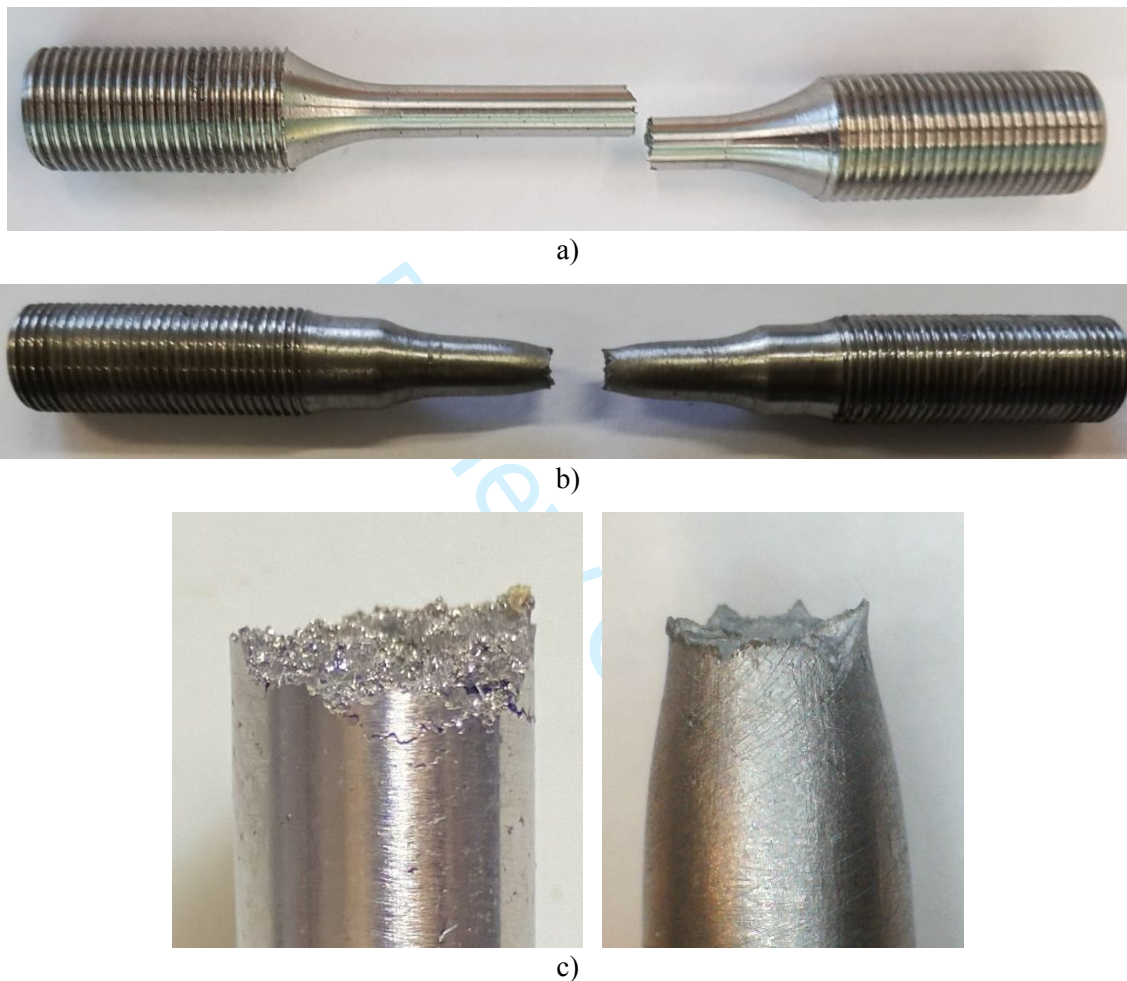


Fig. 5 – Uniaxial tensile specimens: a) SLM (B11); b) conventional (A14); and c) detailed view of fracture surfaces – SLM and conventional, respectively.

4.5 Fatigue tests (SN curves)

Equation 2 is commonly used in the engineering context to correct the fatigue limit stress, σ_{f0} , obtained with polished specimens with 7 mm diameter and without defects ($K_1=K_2=K_3=1$). It considers the effect of surface finish K_1 , the dimension of the specimen K_2 and the presence of defects K_3 , as well as the type of loading applied. When considering cyclic pure axial loads ($R= -1$), it is assumed that the theoretical fatigue limit stress for a steel is calculated using Equation 3³².

$$\sigma'_{f0} = K_1 \cdot K_2 \cdot K_3 \cdot \sigma_{f0} \quad (2)$$

$$\sigma_{f0} = (0.5 \cdot \text{UTS}) \cdot 0.9 \quad (3)$$

For the fatigue tests carried out, eight specimens obtained by conventional method and seven specimens obtained by SLM were used. The SN diagrams resulting from the fatigue tests are shown in Figure 6.

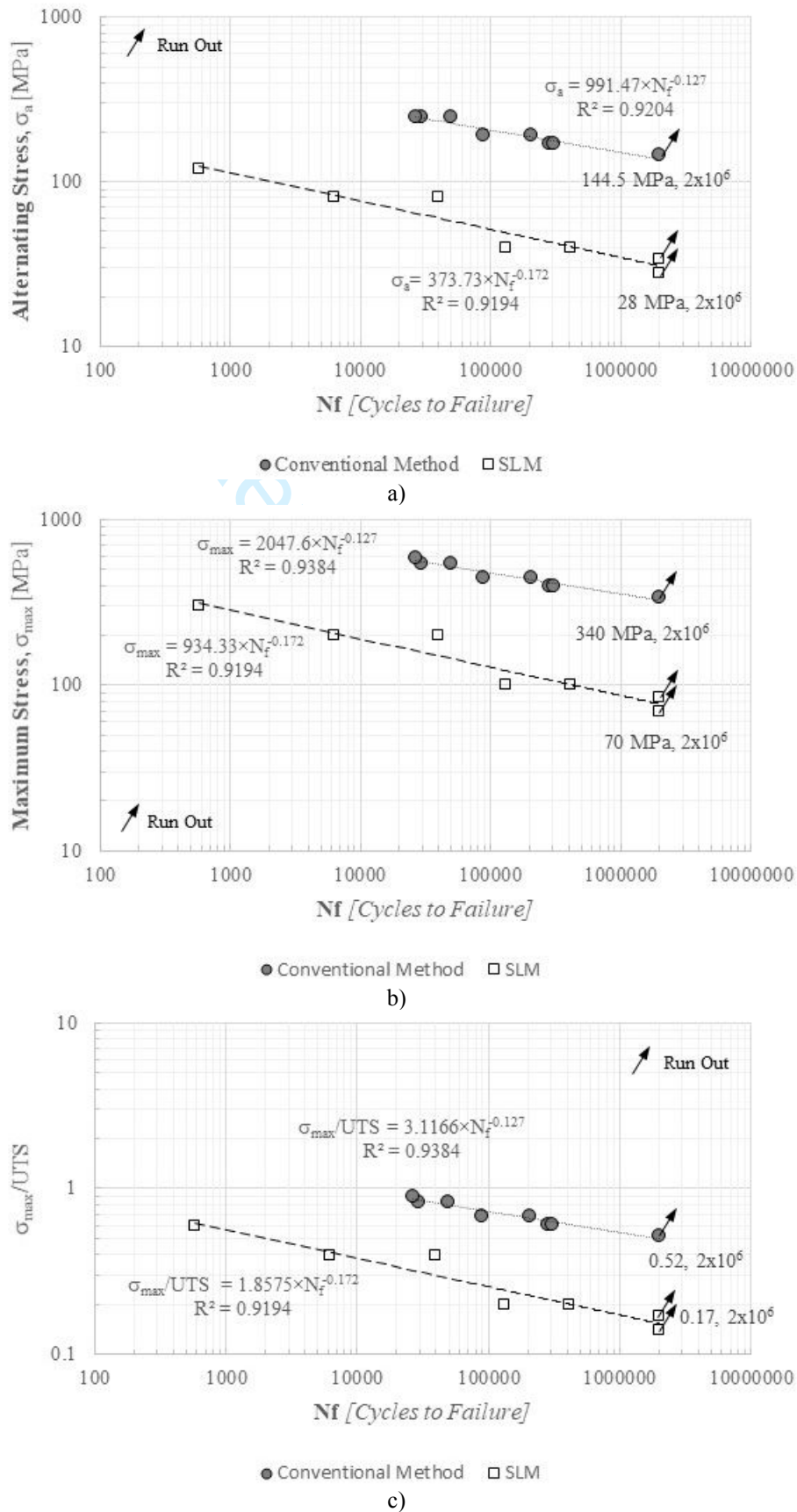


Fig. 6- SN diagrams for AISI H13 steel obtained by conventional manufacture (circles) and SLM manufacture (squares). Load ratio, R, equals 0.2: a) σ_a vs. Nf; b) σ_{max} vs. Nf; and c) σ_{max}/UTS vs. Nf.

As shown in the SN curve represented by Fig. 6a, conventional manufacture samples reached a fatigue limit alternating stress value of 144.5 MPa, and a maximum stress of 340 MPa (Fig. 6b) considering 2×10^6 cycles as run out. Therefore, having into account a non-zero mean stress value of 195.5 MPa, and applying the Goodman's relationship, it was possible to calculate a fatigue limit alternating stress equal to 205 MPa for a load ratio, R, equal to -1. This value is in the same order with the theoretical calculation resultant from the application of Equations 2, 3, and the surface roughness factor, K_1 (0.76), defined in Section 4.1:

$$\sigma'_{fo} = 0.76 \cdot 1 \cdot 1 \cdot 0.9 \cdot (0.5 \times 657) = 224.7 \text{ MPa}$$

Moreover, from a fatigue design point of view (Fig. 6c), it is possible to infer that $\sigma_{max}/UTS=0.51$ for 2×10^6 cycles to failure for the conventional manufacture samples. Besides, the application of the Basquin equation to the SN curve of conventional manufacture samples (Fig.6a) is described by Equation 4.

$$\sigma_a = 991.47 \cdot N_f^{-0.127} \text{ [MPa]} \quad (4)$$

For specimens obtained by SLM, infinite life was obtained for an alternating stress of 34 MPa (Fig. 6a) and a maximum stress value of 85 MPa (Fig. 6b). Using the Goodman's relationship, with a non-zero mean stress value of 51 MPa, a corrected fatigue limit stress value of 38 MPa was obtained. This value is significantly lower than that obtained for conventional manufacture samples, with a reduction in fatigue life of approximately 81%. This is directly related to porosity and lack of fusion noticed in the SLM samples, as described in section 4.2.

Yadollahi *et al.*³³ showed that defects with dimensions between 8-20 μm led to a 57% reduction in fatigue strength for an Inconel 718 alloy. The SLM samples used in the fatigue tests showed internal defects with dimensions between 50-500 μm ; therefore, the reduction in fatigue strength is expected to be even greater. Applying equations 2 and 3, and the surface roughness factor, K_1 (0.9), as defined in section 4.1, a correction factor, K_3 , of approximately 0.19, is obtained due to defects:

$$\sigma'_{fo} = 0.9 \cdot 1 \cdot K_3 \cdot 0.9 \cdot (0.5 \times 503) = 38 \text{ MPa} \therefore K_3 = 0.19$$

Moreover, from a fatigue design point of view (Fig. 6c), it is possible to infer that $\sigma_{max}/UTS=0.17$ for 2×10^6 cycles to failure. Besides, the application of the Basquin equation to the SN curve of SLM manufacture samples (Fig.6a) is described by Equation 5.

$$\sigma_a = 373.73 \cdot N_f^{-0.172} \text{ [MPa]} \quad (5)$$

4.6 SEM analysis

It was possible to carry out an SEM analysis of the fracture surfaces obtained from the tensile and the fatigue tests performed.

The fracture surfaces resulting from the tensile test of specimen A11 (conventional) and specimen C2 (SLM) are shown in Figure 7 for different magnifications. It is possible to observe that the fracture surfaces have different morphologies. The high plastic deformation, typical of a ductile fracture, is visible on the fracture surface of conventional manufacture specimens (A11), as illustrated in Figure 7 c). On the other hand, the low plastic deformation associated with a brittle fracture is illustrated in Figure 7 b). It was also found that the material obtained by conventional methods has a greater

homogeneity compared to those obtained by SLM, as observed in Figure 7 c) and d), respectively. Figure 7 e) and f) allow to visualize metallic powder that has not melted and some particles that have not adhered to each other. This occurrence, together with voids, residual stresses and anisotropic microstructure can affect the overall mechanical behaviour of these components^{34,35}.

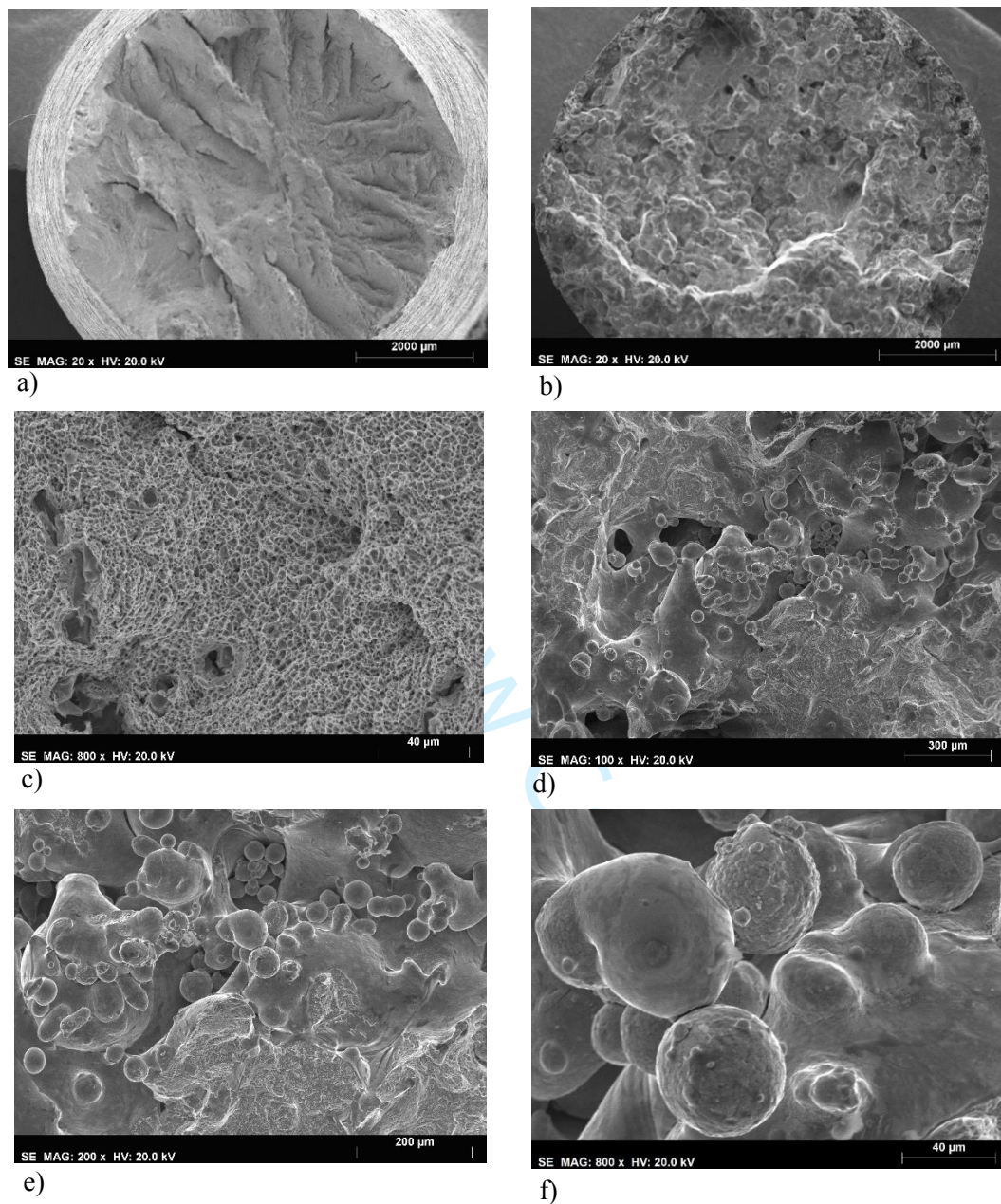


Fig. 7- SEM analysis performed on fracture surfaces of: conventional specimens with different magnifications a) 20x and c) 800x; and SLM specimens with different magnifications: b) 20x; d) 100x; e) 200x and f) 800x, subjected to monotonic tensile test.

Figures 8 a), b), and c) represent the fracture surfaces resulting from the fatigue tests carried out on conventional test specimens (A9, A15 and A5), respectively. In these images, it is possible to see that the fatigue cracks propagated from right to left. The progression/stop lines are more pronounced in Figure 8 a) and b), making it possible to distinguish the propagation and final fracture region easily. The fractures of specimens A9, A15 and A5 occurred when the cracks reached 47%, 58% and 31% of the diameter, respectively. Figure 8 d) shows two initiation points on the outer surface, which gave rise to the specimen failure.

The propagation and the final fracture region's morphology are also distinct, represented in Figure 8 e) and f), respectively. The final fracture region (Figure 8f) has a surface similar to that obtained during the tensile test, as shown in Figure 7 c), characteristic of a ductile fracture. In the fatigue propagation region (Figure 8e), some fatigue striations are visible and secondary cracking, perpendicular to the main crack propagation direction, evidence of a high crack propagation speed and high-stress intensity factor. The mechanism of crack propagation is predominantly transgranular.

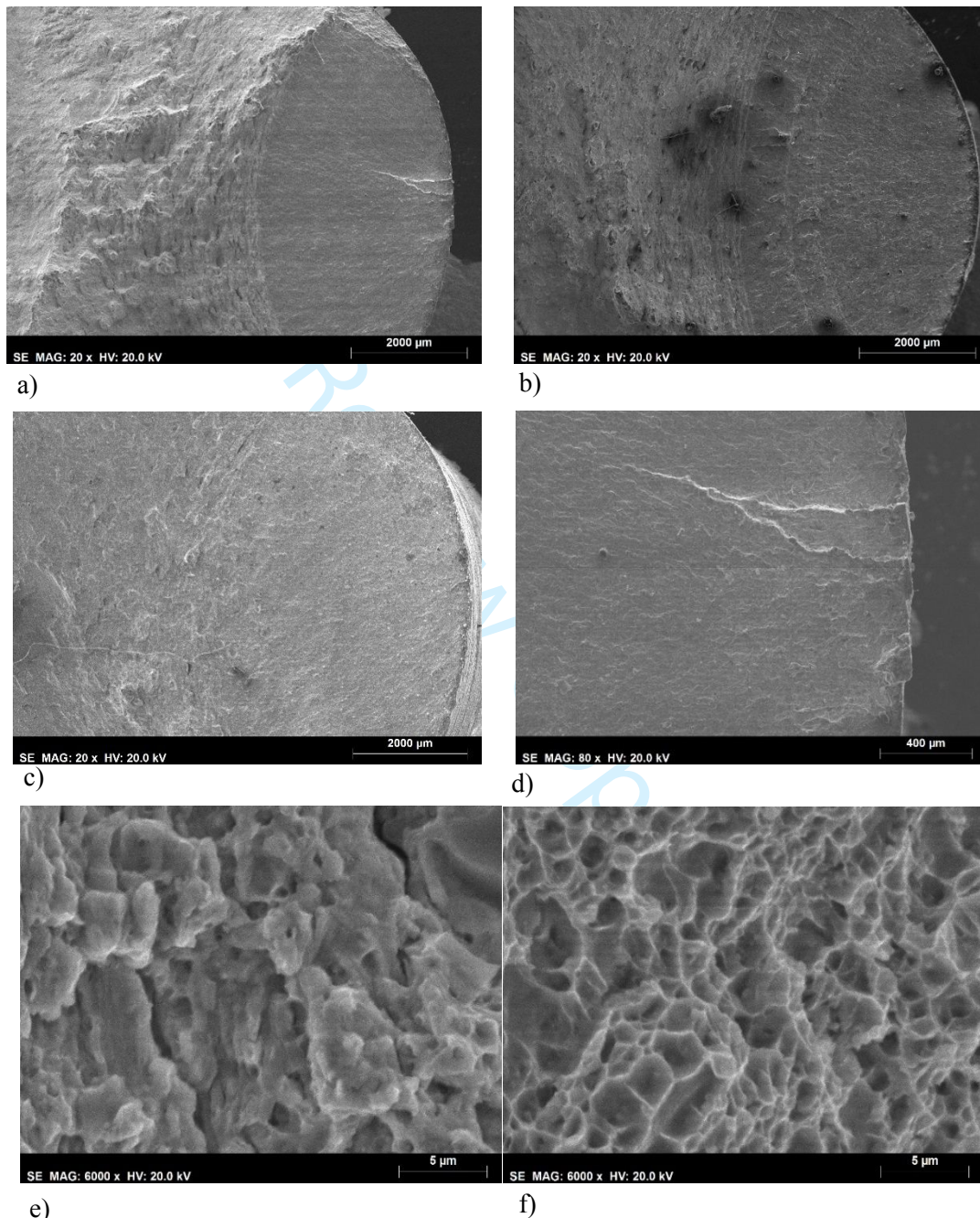
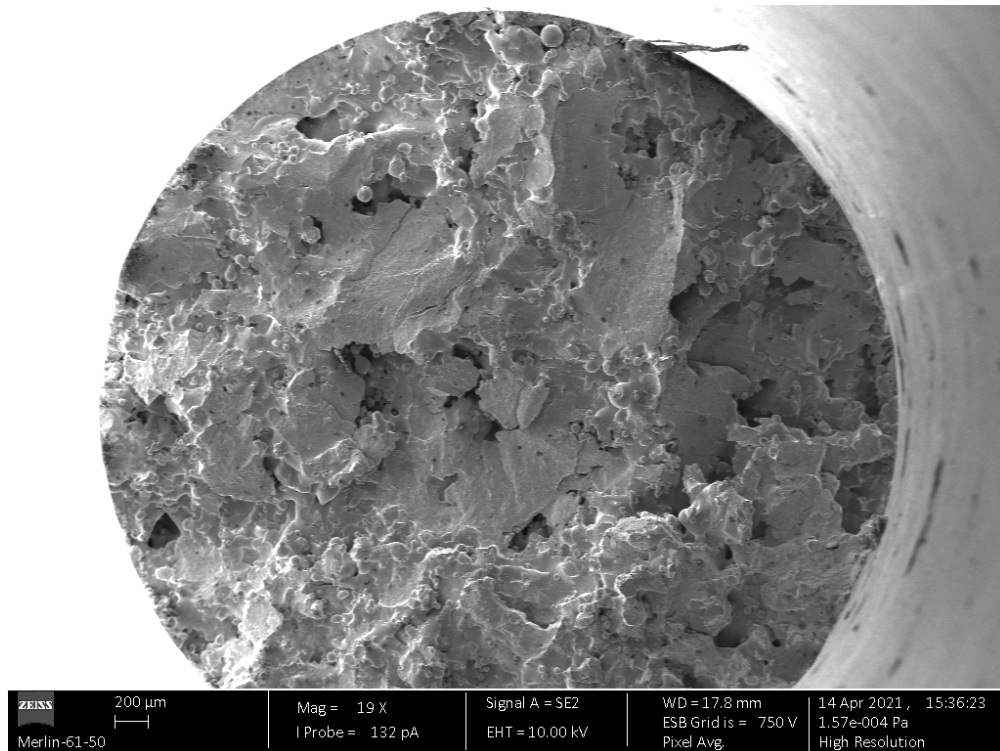


Fig. 8- SEM analysis performed on the fracture surfaces obtained from fatigue tests of conventional specimens for different magnifications: a) 20x; b) 20x; c) 20x; d) 80x; e) Morphology of the crack propagation region and f) final fracture surface.

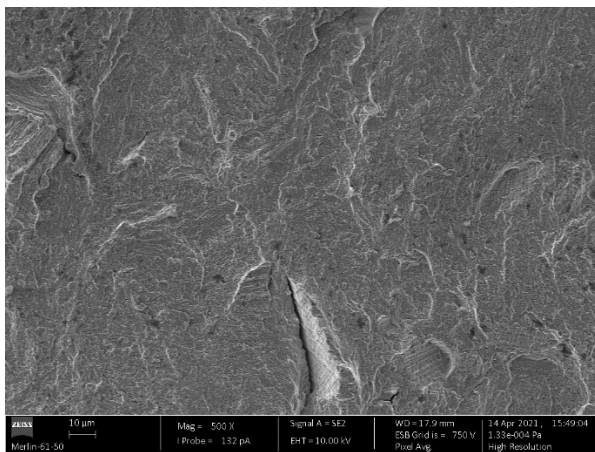
Considering the SLM specimens tested under fatigue loading, some SEM images are presented in Figure 9, and they refer to specimen B5, which revealed a fatigue life of 412 216 cycles. As shown in Figure 9a, the crack nucleation and propagation started at the top of the fracture surface and propagated through the specimen's cross-section, even beyond its centre. Moreover, at the bottom of Figure 9a, a

typical fracture surface is obtained by applying tensile stresses in a remaining area that could not withstand the load applied, which compares with the fracture surface obtained in the uniaxial tensile tests carried out (Fig. 7b). Besides, lack of fusion and porosity are also visible in Figure 9a.

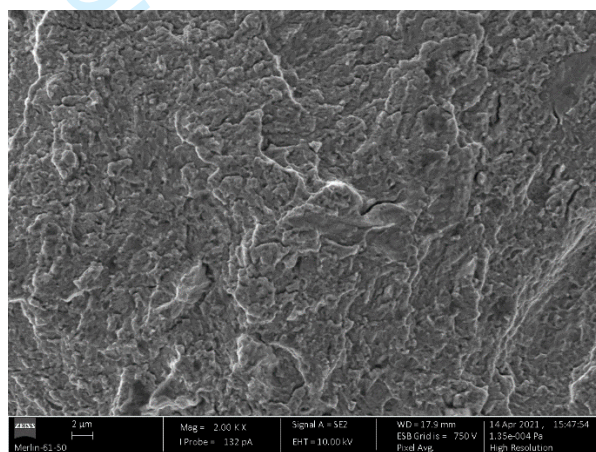
Concerning the fatigue crack propagation region (Fig. 9b and c), it is possible to observe a flat fracture surface, without traces of relevant plastic deformation and with secondary cracking, which reveals the presence of high stress intensity factor values and high fatigue crack growth rates.



a)



b)



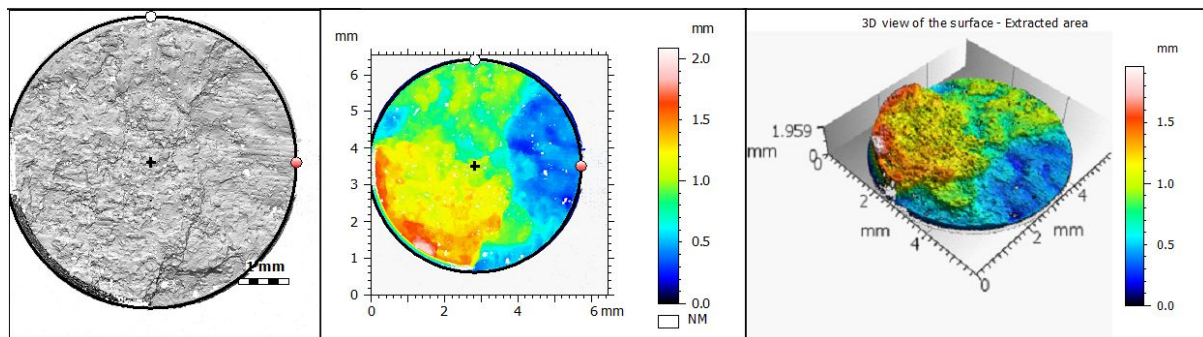
c)

Fig. 9- SEM analysis performed on the fracture surfaces obtained from fatigue tests of SLM specimens for different magnifications: a) 19x; b) 500x; c) 2000x.

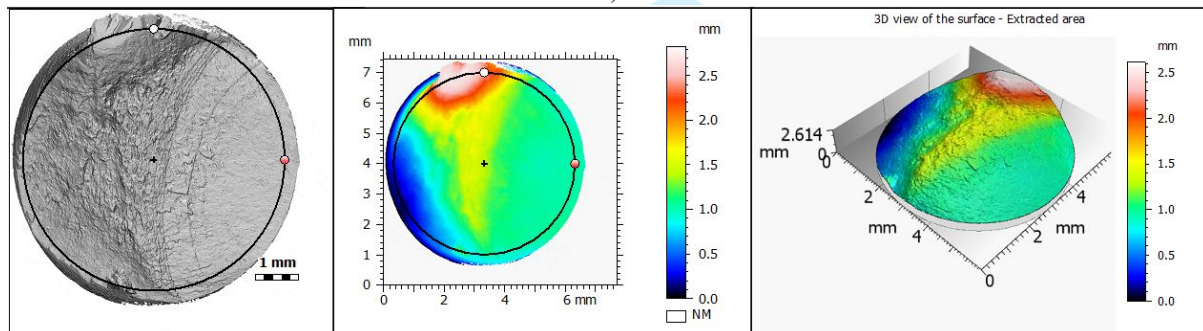
4.7 3D fractography

Comparing the fracture surface topography of the SLM and conventional specimens submitted to fatigue loading, two fracture surfaces are visible in Figure 10. Surface parameters were evaluated via

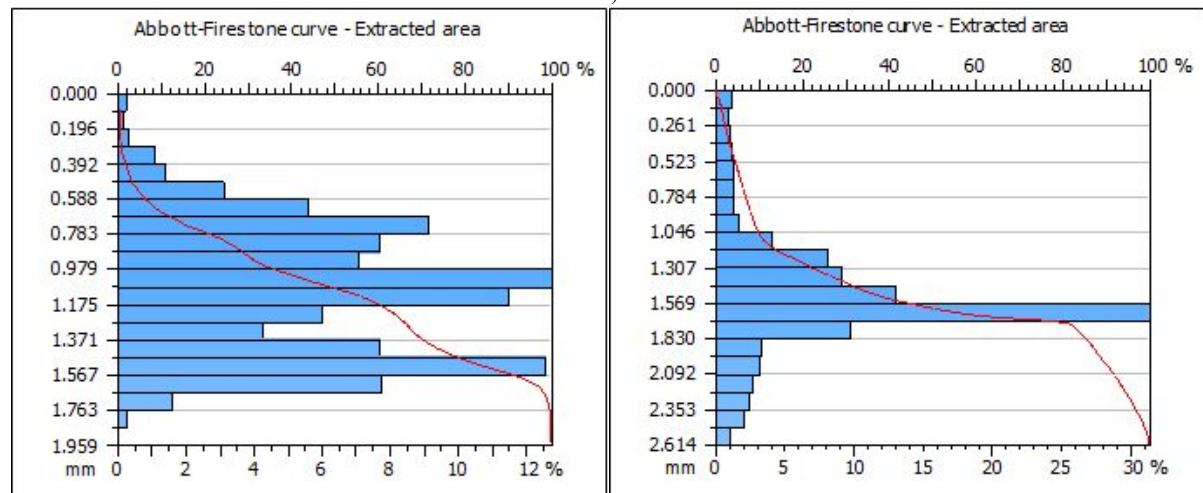
the entire total area method^{36,37}. For SLM, it is a fracture surface with a very irregular morphology (Fig. 10a), similar to that shown in Fig. 7b. The crack started in the area with the lowest level (in blue) from the specimen's outer surface and spread into the interior (Fig. 10a). Because it is a specimen subjected to a high load, which fractured after a reduced number of cycles (580), the propagation region is tiny compared to the final fracture region (identified in green, yellow, and red). The fracture surface of the conventional specimen (Fig. 10b) is more regular, with smoother and more progressive variations of the surface topography from the crack initiation site to the final fracture, reflected in the histogram seen in Fig. 10c on the right. The depth histogram presents the distribution density of the surface data points. The horizontal axis is drawn in per cent of the total population, and the vertical one in depths, followed by the Abbott-Firestone curve plotted in red. It is clear from the Figure 10c that either the histograms or the Abbott-Firestone curves are quite different. For the conventional specimen, we can see a clear peak (at a depth of 1.569) followed by a progressive decrease to both sides, leading to an almost symmetrical distribution. On the contrary, for the SLM specimen, there are no dominant peaks. Instead, we can see a number of depths with similar percentage and only the extreme values are relatively less frequent.



a)



b)



c)

Fig. 10- Fracture surface topography: a) SLM specimen; b) conventional specimen and c) The depth histograms of the fracture surfaces for a SLM specimen and a conventional specimen, respectively. The horizontal axis represents the bearing ratio [%], and the vertical axis represents the depths (measurement unit).

5. Conclusions

With the present work, the determination of the mechanical behaviour of an AISI H13 steel obtained by SLM was carried out and compared with the same steel obtained through conventional manufacturing methods. The objectives initially proposed were fulfilled, being possible to draw the following conclusions:

- Compared to the manufacture by conventional methods, the mechanical properties of the material obtained by SLM are similar to those obtained by the former, except the fatigue strength and the rupture strain;
- For the SLM manufacturing parameters used, the average percentage of pores was about 8% of the cross-section area and lack of fusion was also verified;
- A maximum hardness value of 549 HV was obtained near the outer surfaces of test pieces manufactured using SLM;
- In the uniaxial tensile tests performed on SLM test pieces, a maximum tensile strength (UTS) value of 513 MPa was obtained. Regarding the rupture strain, values below 1% were obtained, resulting in a brittle fracture of the material;
- The fatigue limit stress ($R=-1$) of the material obtained by SLM occurred at an alternating stress of 38 MPa, thus presenting a reduction of 80% compared with AISI H13 steel obtained by conventional methods (205 MPa). This is directly related to porosity and lack of fusion noticed in the SLM samples (8%), and, due to that, a fatigue limit correction factor of about 0.19 should apply in the design stage of any additively component with such level of defects;
- From a fatigue design point of view, it was possible to infer that $\sigma_{\max}/UTS=0.51$ for 2×10^6 cycles to failure for the conventional manufacture samples;
- From a fatigue design point of view, it was possible to infer that $\sigma_{\max}/UTS=0.17$ for 2×10^6 cycles to failure for the SLM specimens tested. Therefore, the use of additively manufactured components with such an average percentage of pores (8%) is only acceptable for non-critical applications submitted to low service fatigue loading.

Acknowledgments

Authors acknowledge Fundação para a Ciência e a Tecnologia (FCT-MCTES) for its financial support via the project UIDB/00667/2020 (UNIDEMI) and project UIDB/00285/2020 (CEMMPRE). Authors also acknowledge Science and Technology Park in Opole for enabling access to test equipment.

Data Availability Statement

The data that support the findings of this study are available from the corresponding author upon reasonable request.

References

- [1] Zhang Y, Wu L, Guo X, Kane S, Deng Y, Jung YG et al.. Additive manufacturing of metallic materials: A review. *Journal of Materials Engineering and Performance*. 2018; 27: 1–13.
- [2] Zenou M, Grainger L. *Additive manufacturing of metallic materials*. Elsevier Inc., 2018.
- [3] Zebrowski R, Walczak M, Korga A, Iwan M, Szala M. Effect of Shot Peening on the Mechanical Properties and Cytotoxicity Behaviour of Titanium Implants Produced by 3D Printing Technology, *Journal of Healthcare Engineering*, 2019; Volume 2019: Article ID 8169538.
- [4] Buican GR, Oancea G, Martins RF. Study on SLM manufacturing of teeth used for dental tools testing, In: Oancea G, Drăgoi MV, eds. *Proceedings of THE 4th INTERNATIONAL CONFERENCE ON COMPUTING AND SOLUTIONS IN MANUFACTURING ENGINEERING - CoSME'16*. Brasov: MATEC Web of Conferences, 94; 2017:

- 1
2
3 <http://dx.doi.org/10.1051/mateconf/20179403002>
- 4 [5] Afkhami S, Dabiri M, Alavi SH, Björk T, Salminen A. Fatigue characteristics of steels manufactured by selective
5 laser melting, *Int. J. Fatigue*, 2019; 122: 72–83.
- 6 [6] Yan J, Song H, Dong Y, Quach WM, Yan M. High strength (~2000 MPa) or highly ductile (~11%) additively
7 manufactured H13 by tempering at different conditions, *Mater. Sci. Eng. A*, 2020, doi: 10.1016/j.msea.2019.138845.
- 8 [7] Mazur M, Brincat P, Leary M, Brandt M. Numerical and experimental evaluation of a conformally cooled H13 steel
9 injection mould manufactured with selective laser melting, *Int. J. Adv. Manuf. Technol.*, 2017; 93: 881–900.
- 10 [8] Hölker-Jäger R, Tekkaya AE. Additive manufacture of tools and dies for metal forming, *Laser Addit. Manuf. Mater.
11 Des. Technol. Appl.*, 2017; 1: 439–464.
- 12 [9] Additive Manufacturing Applications Market Analysis: Metal Additive Manufactured Parts Produced. SmarTech
13 Analysis, 11 2019. SKU: SMP-AM-AMA-1119.
- 14 [10] Xue L. *Laser Consolidation—A Rapid Manufacturing Process for Making Net-Shape Functional Components*,
15 Second Edition. Elsevier Ltd., 2018.
- 16 [11] ASM International, ASM Metals Handbook, Volume 1: Properties and selection: Irons Steels and High Performance
17 Alloys. 1990.
- 18 [12] Yeşildal R. The Effect of Heat Treatments on the Fatigue Strength of H13 Hot Work Tool Steel, 2018; pp. 1–13, doi:
19 10.20944/PREPRINTS201812.0226.V1.
- 20 [13] Kurzynowski T, Chlebus E, Kuźnicka B, Reiner J. Parameters in selective laser melting for processing metallic
21 powders, *High Power Laser Mater. Process. Lasers, Beam Deliv, Diagnostics and Appl.*, 2012; 8239, doi:
22 10.1117/12.907292.
- 23 [14] Laakso P, Riipinen T, Laukkanen A, Andersson T, Jokinen A, Revuelta A *et al.*. Optimization and simulation of SLM
24 process for high density H13 tool steel parts, *Phys. Procedia*, 2016; 83: 26–35.
- 25 [15] Lee J, Choe J, Park J, Yu J, Kim S, Doo I. Materials Characterization Microstructural effects on the tensile and
26 fracture behavior of selective laser melted H13 tool steel under varying conditions, *Mater. Charact.*, 2019; 155: p.
27 109817.
- 28 [16] Deirmina F, Peghini N, AlMangour B, Grzesiak D, Pellizzari M. Heat treatment and properties of a hot work tool
29 steel fabricated by additive manufacturing, *Mater. Sci. Eng. A*, 2019; 753: 109–121.
- 30 [17] Nagahama T, Mizoguchi T, Yonehara M, Kyogoku H. The Porosity and Mechanical Properties of H13 Tool Steel
31 Processed by High-speed Selective Laser Melting. Proceedings of the 30th Annual International Solid Freeform
32 Fabrication Symposium – An Additive Manufacturing Conference; 2019: 677–683.
- 33 [18] Dörfert R, Zhang J, Clausen B, Freife H, Schumacher J, Vollertsen F. Comparison of the fatigue strength between
34 additively and conventionally fabricated tool steel 1.2344, *Addit. Manuf.*, 2019; 27: 217–223.
- 35 [19] SLM Solutions – 3D Metals: Discover the variety of metal powders. [www.slm-
36 solutions.com/fileadmin/Content/Powder/MDS/MDS_Fe-Alloy_H13_0219_EN.pdf](http://www.slm-solutions.com/fileadmin/Content/Powder/MDS/MDS_Fe-Alloy_H13_0219_EN.pdf) (accessed on June 3rd, 2021)
- 37 [20] ASTM E384-17, Standard Test Method for Microindentation Hardness of Materials, ASTM International, West
38 Conshohocken, PA, 2017.
- 39 [21] Japan Society of Mechanical Engineers, Standard Method of Statistical Fatigue Testing. JSME 1981; S:002-1981.
- 40 [22] Macek W, Branco R, Szala M, Marciniak Z, Ulewicz R, Sczygiol N *et al.*. Profile and Areal Surface Parameters for
41 Fatigue Fracture Characterisation, *Materials* 2020, 2020; 13: 3691
- 42 [23] ASM International, Elements of Metallurgy and Engineering Alloys: Chapter 14: Fatigue, Editor F. C. Campbell, pp.
43 243–265, 2008.
- 44 [24] Koneshlou M, Asl KM, Khomamizadeh F. Effect of cryogenic treatment on microstructure, mechanical and wear
45 behaviors of AISI H13 hot work tool steel, *Cryogenics (Guildf.)*, 2011; 51: 55–61.
- 46 [25] Dzukey GA, Yang K, Wang Q, Zhuang B, Hou W. Porosity, Hardness, Friction and Wear Performance Analysis of
47 H13 SLM-Formed Samples, *J. Mater. Eng. Perform.*, 2020; 29: 4957–4966.
- 48 [26] ASM Specialty Handbook: Tool Materials, Editor Joseph R. Davis, 1995, ASM International
- 49 [27] H13 Tool Steel | 1.2344 | SKD61 Hot Work Steel - Otai Special Steel. [Online]. Available:
50 <http://www.astmsteel.com/product/h13-tool-steel-x40crmov5-1-sk61-hot-work-steel/> (accessed on June 3rd, 2021).
- 51 [28] Mertens R, Vrancken B, Holmstock N, Kinds Y, Kruth JP, Van Humbeeck J. Influence of powder bed preheating on
52 microstructure and mechanical properties of H13 tool steel SLM parts, *Phys. Procedia*, 2016; 83: 882–890.
- 53 [29] Kelly CN, Evans NT, Irvin CW, Chapman SC, Gall K, Safranski DL. The effect of surface topography and porosity
54 on the tensile fatigue of 3D printed Ti-6Al-4V fabricated by selective laser melting, *Mater. Sci. Eng. C*, 2019; 98:
55 726–736.
- 56 [30] Yadroitsava I, Yadroitsev I. Effects of defects on mechanical properties in metal additive manufacturing : A review
57 focusing on X-ray tomography insights, *Mater. Des.*, 2020; 187: 108385.
- 58 [31] Wilson-Heid AE, Novak TC, Beese AE. Characterization of the Effects of Internal Pores on Tensile Properties of

- 1
2
3 Additively Manufactured Austenitic Stainless Steel 316L, *Experimental Mechanics*, 2019; 59: 793–804.
- 4 [32] Lee YL, Pan J, Hathaway R, Barkey M. *Fatigue Testing and Analysis – Theory and practice*, 1st edition, 416 pages,
5 Butterworth-Heinemann, Elsevier, 2004
- 6 [33] Yadollahi A, Mahtabi MJ, Khalili A, Doude HR, Newman JC. Fatigue life prediction of additively manufactured
7 material: Effects of surface roughness, defect size, and shape, *Fatigue Fract. Eng. Mater. Struct.*, 2018; 41: 1602–
8 1614.
- 9 [34] Solberg K, Guan S, Razavi SMJ, Welo T, Chan KC, Berto F. Fatigue of additively manufactured 316L stainless steel:
10 The influence of porosity and surface roughness. *Fatigue Fract. Eng. Mater. Struct.*, 2019; 42: 2043-2052.
- 11 [35] Fergani O, Berto F, Welo T, Liang SY. Analytical modelling of residual stress in additive manufacturing. *Fatigue*
12 *Fract. Eng. Mater. Struct.* 2017; 40: 971-978.
- 13 [36] Macek W, Branco R, Trembacz J, Costa JD, Ferreira JAM, Capela C. Effect of multiaxial bending-torsion loading on
14 fracture surface parameters in high-strength steels processed by conventional and additive manufacturing,
15 *Engineering Failure Analysis*, 2020; 118: 104784.
- 16 [37] Macek W. Post-failure fracture surface analysis of notched steel specimens after bending-torsion fatigue, *Engineering*
17 *Failure Analysis*, 2019; 105: 1154-1171.
18
19
20
21
22
23
24
25
26
27
28
29
30
31
32
33
34
35
36
37
38
39
40
41
42
43
44
45
46
47
48
49
50
51
52
53
54
55
56
57
58
59
60

Review Copy